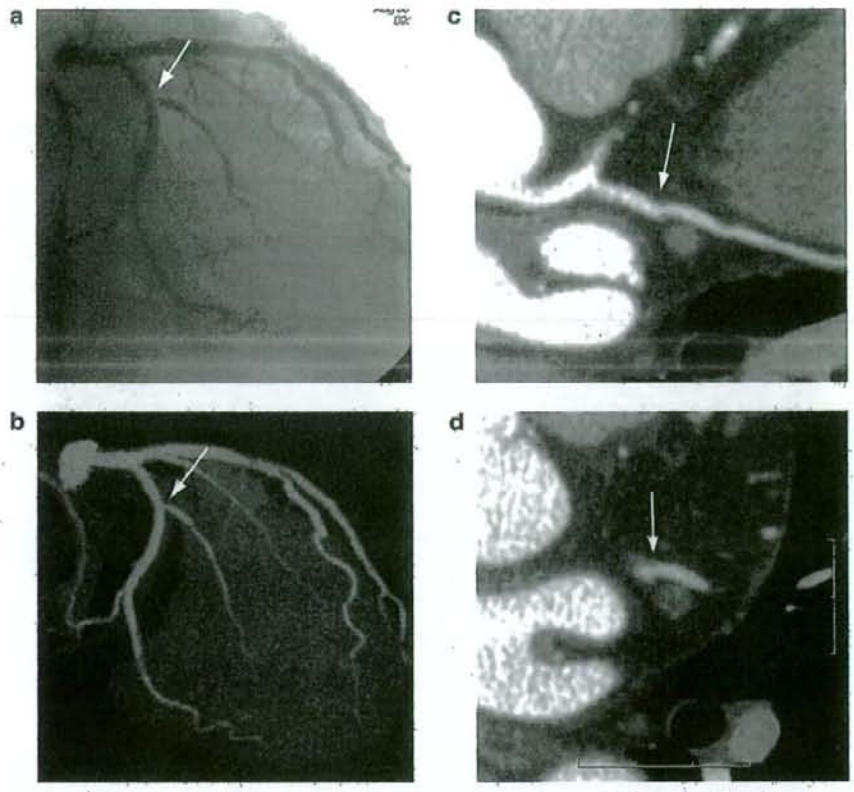

Figure 4. A 63-year-old man with a significant stenosis located in the just proximal portion of the obtuse marginal branch on the invasive angiogram (**a**: arrow). This lesion was diagnosed as >50% stenosis on the angiographic view image (**b**: arrow), but was judged to be <50% stenoses (false negative) with the conventional methods (**c**: arrow) and on the axial images (**d**: arrow).

Table 3. Results of Quantitative Coronary Angiography for False-Positive Lesions of Each Viewing Method

	Lesions with no severe calcification			Lesions with severe calcification			Total
	Mild stenosis	Trivial stenosis	No stenosis	Mild stenosis	Trivial stenosis	No stenosis	
Angiographic view image	7	1	1†	5	3	0	17
Conventional methods	3	1	0	4	3	0	11
Axial images alone	25	1	4	4	3	0	37

Mild stenosis: 26–50%; trivial stenosis: 1–25% stenoses.
†Muscular bridge.

Results

Of 208 segments >1.5 mm in diameter, 196 segments were included. Among the 12 segments excluded, 10 had stents and 2 were segments with a discontinuous area because of premature beat. QCA showed significant coronary artery stenoses (ie, 1 or more stenoses >50%) in 22% (44/196) of the segments. All coronary segments >1.5 mm in diameter and seen on the axial images were also identified by the conventional methods and on the AGV image.

Diagnostic Accuracy of Each Viewing Method

Table 1 shows the results of the 3 viewing methods for lesion detection by coronary artery segment. In the comparison of the AGV image and conventional methods, sensitivity was the same (98%) and there was no significant difference in accuracy (P>0.05: 91% with AGV image and 94% with conventional methods) (**Figure 2**). The accuracy of the AGV image was significantly higher compared with axial images alone (P<0.05).

False-Negative (FN) Lesions of Each Viewing Method

The location of the FN lesion differed among the viewing methods (**Table 2**).

With the AGV image, a FN lesion was located just proximal portion to the left circumflex artery where the vessel

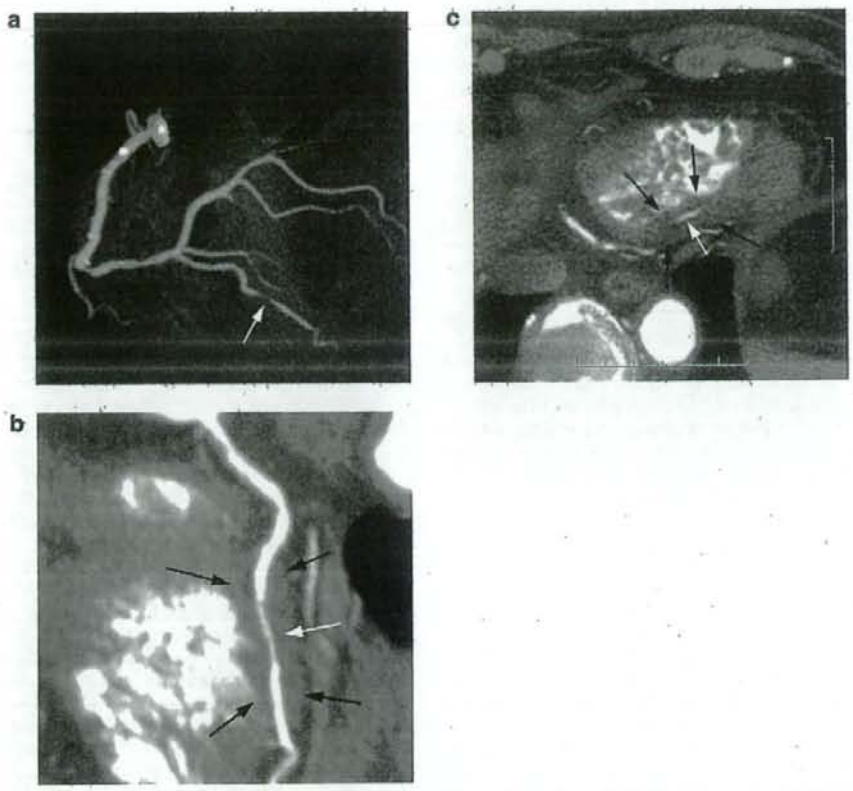

Figure 5. A 73-year-old man with a myocardial bridge in the poster descending branch. The lesion was judged as >50% stenosis on the angiographic view (a: arrow). With the conventional methods (b) and on the axial images (c), this lesion (white arrow) seemed to be >50% stenosis, but was judged to be a myocardial bridge not a stenotic lesion because of plaque, because myocardium (black arrows) was seen surrounding the lesion.

branched out from the mid-portion of the stent (**Figure 3**). This may have been a stent artifact, which appears to "bloom" the outer margin of the stent, hiding lesions in the just proximal portion from view.

With the conventional methods, a FN lesion was located in the just proximal portion of the obtuse marginal artery (**Figure 4**). This type of lesion can appear stenotic using projection methods such as the AG view and QCA, but as seen with the conventional methods, it may in fact be non-stenotic. However, if QCA is used as the gold standard, the result will be an AGV image true-positive and conventional false-negative.

With the axial images alone, 5 of 6 FN lesions were located in the segment running horizontal to the axial section, and the remaining 1 was the same as the FN lesion in the AGV image.

False-Positive (FP) Lesions of Each Viewing Method

The FP lesions for each viewing method varied with the results of QCA (**Table 3**). The FP lesions were divided into 2 categories: with and without severe calcification.

Lesions With Severe Calcification The total number of lesions with severe calcification was 24. On the AGV image, 5 of the 8 FP lesions with severe calcification were mild stenoses (26–50%), and 3 were trivial (1–25%). With the conventional methods and on the axial images alone, 4 of 7 FP lesions were mild stenoses and 3 were trivial stenoses. The "blooming" artifact of calcification was considered to cause the overestimation of mild or trivial stenoses. One severe calcification of a mild stenosis was FP only on the AGV image, and true-positive with the conventional methods and the axial images alone.

Lesions With No Severe Calcification The total number of lesions with no severe calcification was 172. On the AGV image, 7 of the 9 FP lesions with no severe calcification were mild stenoses, 1 was a trivial stenosis, and the other was a non-stenosis on QCA. Thus, the main cause of FP lesions on the AGV image was overestimation of mild stenoses as >50% stenoses. One trivial-stenotic lesion was accompanied by protruding moderate calcification (occupying less than 50% diameter), thus the blooming artifact of calcification was considered to cause the overestimation of trivial stenoses as >50% stenoses on the AGV image. One non-stenotic lesion on QCA was a myocardial bridge (**Figure 5**). This lesion was also viewed as stenotic by the conventional methods and on the axial images alone. However, those methods demonstrated the myocardium surrounding the vessel, and thus enabled the correct diagnosis of myocardial bridge not stenotic lesion because of plaque.

With the conventional methods, 3 of the 4 FP lesions were mild stenoses on QCA, and the other was a trivial stenosis (same as with the FP lesion on the AGV image ; the lesion was accompanied by protruding moderate calcification).

On the axial images alone, 25 of the 30 FP lesions were mild stenoses, 1 was a trivial stenosis, and 4 were non-stenoses on QCA. The number (n=30) of FP was much more than on the AGV images (n=9) or with the conventional methods (n=4). This was retrospectively considered to be related to evaluation of lesions located in the segment running horizontal to the axial section, and that diffuse concentric plaque with positive remodeling in all length of segment is more difficult to determine on axial images compared with other methods. Among the 30 FP lesions on the axial images alone, 14 were located in the segment running horizontal to the axial section (horizontal lesion), and 4 were diffuse concentric plaque with positive remodeling in all length of segment (concentric lesion). Among the 9 FP lesions on the AGV images, only 1 was a horizontal lesion and 0 with the conventional methods, and no concentric lesions with either method.

Discussion

The axial image is the basic clinical reference for detailed image analysis. However, because of the complex course of the coronary artery, interpretation of axial images may be difficult and the use of post-processing techniques enables investigators to better understand the complex coronary artery anatomy and abnormalities. There have been several studies of the use of various post-processing methods for CT CAG and according to their results, a combination of various viewing methods gives the highest sensitivity, and was used in most of the studies[10–12] Thus, we compared the diagnostic accuracy of the AGV image with a combination of various viewing methods, and also with axial images alone.

We found significant coronary artery stenoses were detected on the AGV image with a sensitivity of 98% and specificity of 89%, and with 98% and 93%, respectively, by the conventional methods. Our findings are comparable with those from recent reports of the accuracy of 64-slice CT for the detection of coronary artery stenoses (sensitivity: 93–99%, specificity: 86–97% and NPV 98–99%) analyzed by a combination of conventional methods[2–4,13–15] In the present study, there was only 1 FN finding on the AGV image, which was a very rare lesion located in the just proximal portion of the left circumflex artery where the vessel branches out from the mid-portion of the stent, and the sensitivity of the AGV image was the same as that with the conventional methods. Our results show that the AGV image is a reliable method of identifying significant stenoses.

The accuracy of the AGV image, as with the conventional methods, was significantly higher compared with the axial images alone. Correct diagnosis was more difficult with the axial images than the other viewing methods in the lesions located in the segment running horizontal to the axial section. Diffuse concentric plaque with positive remodeling also has a tendency to be incorrectly viewed as stenotic on axial images, possibly because the reference diameter (vessel diameter in non-diseased artery immediately proximal to the lesion) of these lesions is not measurable on the axial image. For evaluation of these types of lesions, the post-processing image is better suited, although this is a pilot study and thus will require further evaluation.

In a previous study, the sensitivity of the axial image (73.4%) was reported to be superior to virtual angioscopic (49.1%), VR (43.0%), and MPR images (46.8%) from 4-section multidetector CT[8] It seems that axial images are less susceptible to motion artifacts, and the poor results obtained for MPR may have been because strictly orthogonal reformation were obtained only along the centerline of virtual endoscope images and, consequently, segments not captured with VE were also not displayed on the MPRs[16] The 64-detector row CT decreased the frequency of motion artifact, and because the post-processing image can be created in any angle without restrictions, a higher diagnostic accuracy can be expected than with axial images. Another recent study reported high diagnostic accuracy of axial images (sensitivity of 89% and specificity of 89% in assessable arteries and an overall accuracy of 88%) using 16-section multidetector CT[16] This high accuracy may be related to per-artery analysis, not per-segment analysis as in our study, and exclusion of side branches from analysis.

The AGV image is a noninvasive overview of all the coronary arteries and accurately shows the distribution of coronary stenoses in 1 set of images that is understandable by third parties. This would be useful in several situations. First, it would be useful for explaining the severity of disease to the patient. Second, the AGV image can be divided into right and left coronary artery, resembling the images from invasive CAG, which enables viewing the lesions from the same angle as with QCA, and detecting the best angle of the lesion prior to percutaneous coronary intervention would be useful in the discussion of the treatment strategy in conference.

The major drawback of the AGV image is that the specificity for coronary stenosis detection compared with conventional methods was lower, the main cause being overestimation of mild stenoses on QCA as >50% stenoses on the AGV image. Previous studies report that MIP can overestimate the degree of stenosis[17–21] so because the AGV image is a MIP image, the lower specificity is understandable. However, this drawback is considered not to be a problem, because the most important factor for the identification of stenotic lesions is high sensitivity.

It is usually difficult to accurately assess the degree of stenosis of lesions with severe calcification[1–4] In our study, 8 of 24 (33%) lesions with severe calcification were FP on the AGV image, and 7 of 24 (29%) lesions were FP with the conventional methods and on the axial images alone. Further study in a larger number is necessary to clarify the characteristics of each viewing method for the evaluation of lesions with severe calcification.

Study Limitations

First, this was a pilot study and thus the number of subjects was small. Second, QCA was used as the gold standard, but it has its imperfections; stenotic lesions may be missed.

Conclusion

The AGV image shows promise as a reliable post-processing method of identifying coronary artery stenoses. Because the AGV image demonstrates coronary lesions in the 1 image, it would be useful for explaining the severity of disease to the patient, and for discussing the treatment strategy in conference.

References

1. Ropers D, Baum U, Pohle K, Anders K, Ulzheimer S, Ohnesorge B, et al. Detection of coronary artery stenoses with thin-slice multi-detector row spiral computed tomography and multiplanar reconstruction. *Circulation* 2003; **107:** 664–666.
2. Raff GL, Gallagher MJ, O'Neill WW, Goldstein JA. Diagnostic accuracy of noninvasive coronary angiography using 64-slice spiral computed tomography. *J Am Coll Cardiol* 2005; **46:** 552–557.
3. Mollet NR, Cademartiri F, van Mieghem CA, Runza G, McFadden EP, Baks T, et al. High-resolution spiral computed tomography coronary angiography in patients referred for diagnostic conventional coronary angiography. *Circulation* 2005; **112:** 2318–2323.
4. Goldstein JA, Gallagher MJ, O'Neill WW, Ross MA, O'Neil BJ, Raff GL. A randomized controlled trial of multi-slice coronary computed tomography for evaluation of acute chest pain. *J Am Coll Cardiol* 2007; **49:** 863–871.
5. Calhoun PS, Kuszyk BS, Heath DG, Carley JC, Fishman EK. Three-dimensional volume rendering of spiral CT data: Theory and method. *Radiographics* 1999; **19:** 745–764.
6. Feyter PJ, Krestin GP. Image post-processing. *In*: Feyter PJ, Krestin GP, editors. Computed tomography of the coronary arteries. New York: Taylor & Francis; 2005. 27–46.
7. Jinzaki M, Sato K, Tanami Y, Yamada M, Kuribayashi S, Anzai T, et al. Novel method of displaying coronary CT angiography: Angiographic view. *Circ J* 2006; **70:** 1661–1662.
8. Jinzaki M, Yamada M, Sato K, Tanami Y, Anzai T, Sasaki K, et al. Overview image of the lumen and vessel wall in coronary CT angiography: Plaque-loaded angiographic view. *Circ J* 2008; **72:** 671–673.
9. Yamada M, Jinzaki M, Kuribayashi S, Sato K, Tanami Y, Fukumoto K, et al. Novel post-processing image for the visualization of coronary sinus by multidetector-row computed tomography before cardiac resynchronization therapy: Edge-enhanced image. *Circ J* 2008; **72:** 487–488.
10. Pannu HK, Flohr TG, Corl FM, Schoepf UJ. Current concepts in multidetector row CT evaluation of the coronary arteries: Principles, techniques, and anatomy. *Radiographics* 2003; **23:** S111–S125.
11. Ferencik M, Ropers D, Abbara S, Cury RC, Hoffmann U, Nieman K, et al. Diagnostic accuracy of image postprocessing methods for the detection of coronary artery stenoses by using multidetector CT. *Radiology* 2007; **243:** 696–702.
12. Pugliese F, Mollet NR, Runza G, van Mieghem C, Meijboom WB, Malagutti P, et al. Diagnostic accuracy of non-invasive 64-slice CT coronary angiography in patients with stable angina pectoris. *Eur Radiol* 2006; **16:** 575–582.
13. Ropers D, Rixe J, Anders K, Küttner A, Baum U, Bautz W, et al. Usefulness of multidetector row spiral computed tomography with 64-×0.6-mm collimation and 330-ms rotation for the noninvasive detection of significant coronary artery stenoses. *Am J Cardiol* 2006; **97:** 343–348.
14. Vanhoenacker PK, Heijenbrok-Kal MH, Van Heste R, Decramer I, Van Hoe LR, Wijns W, et al. Diagnostic performance of multidetector CT angiography for assessment of coronary artery disease: Meta-analysis. *Radiology* 2007; **244:** 419–428.
15. Achenbach S, Moshage W, Ropers D, Bachmann K. Curved multiplanar reconstructions for the evaluation of contrast-enhanced electron beam CT of the coronary arteries. *Am J Roentgenol* 1998; **170:** 895–899.
16. Vogl TJ, Abolmaali ND, Diebold T, Engelmann K, Ay M, Dogan S, et al. Techniques for the detection of coronary atherosclerosis: Multidetector row CT coronary angiography. *Radiology* 2002; **223:** 212–220.
17. Lu B, Dai RP, Bai H, He S, Jing BL, Jiang SL, et al. Coronary artery stenoses: A phantom study using contrast enhanced three-dimensional electron beam tomography. *Clin Imaging* 2001; **25:** 95–100.
18. Uchino A, Kato A, Kudo S. CT angiography using electron-beam computed tomography (EBCT): A phantom study. *Radiat Med* 1997; **15:** 273–276.
19. Brink JA, Lim JT, Wang G, Heiken JP, Deyoe LA, Vannier MW. Technical optimization of spiral CT for depiction of renal artery stenosis: In vitro analysis. *Radiology* 1995; **194:** 157–163.
20. Dillon EH, van Leeuwen MS, Fernandez MA, Eikelboom BC, Mali WP. CT angiography: Application to the evaluation of carotid artery stenosis. *Radiology* 1993; **189:** 211–219.
21. Rubin GD, Dake MD, Napel S, Jeffrey RB Jr, McDonnell CH, Sommer FG, et al. Spiral CT of renal artery stenosis: Comparison of three-dimensional rendering techniques. *Radiology* 1994; **190:** 181–189.

Variability of Repeated Coronary Artery Calcium Scoring and Radiation Dose on 64- and 16-Slice Computed Tomography by Prospective Electrocardiographically-triggered Axial and Retrospective Electrocardiographically-gated Spiral Computed Tomography: A Phantom Study[1]

Jun Horiguchi, MD, Masao Kiguchi, RT, Chikako Fujioka, RT, Ryuichi Arie, RT, Yun Shen, RT, Kenichi Sunasaka, RT
Toshiro Kitagawa, MD, Hideya Yamamoto, MD, Katsuhide Ito, MD

Rationale and Objectives. We sought to compare coronary artery calcium (CAC) scores, the variability and radiation doses on 64- and 16-slice computed tomography (CT) scanners by both prospective electrocardiographically (ECG)-triggered and retrospective ECG-gated scans.

Materials and Methods. Coronary artery models ($n = 3$) with different plaque CT densities (~240 Hounsfield units [HU], ~600 HU, and ~1000 HU) of four sizes (1, 3, 5, and 10 mm in length) on a cardiac phantom were scanned three times in five heart rate sequences. The tube current-time products were set to almost the same on all four protocols (32.7 mAs for 64-slice prospective and retrospective scans, 33.3 mAs for 16-slice prospective and retrospective scans). Slice thickness was set to 2.5 mm to keep the radiation dose low. Overlapping reconstruction with a 1.25-mm increment was applied on the retrospective ECG-gated scan.

Results. The CAC scores were not different between the four protocols (one-factor analysis of variance: Agatston, $P = .32$; volume, $P = .19$; and mass, $P = .09$). Two-factor factorial analysis of variance test revealed that the interscan variability was different between protocols ($P < .01$) and scoring algorithms ($P < .01$). The average variability of Agatston/volume/mass scoring and effective doses were as follows: 64-slice prospective scan: 16%/15%/11% and 0.5 mSv; 64-slice retrospective scan: 11%/11%/8% and 3,7 mSv; 16-slice prospective scan: 20%/18%/13% and 0.6 mSv; and 16-slice retrospective scan: 16%/15%/11% and 2.9 to 3.5 mSv (depending on the pitch).

Conclusion. Retrospective ECG-gated 64-slice CT showed the lowest variability. Prospective ECG-triggered 64-slice CT, with low radiation dose, shows low variability on CAC scoring comparable to retrospective ECG-gated 16-slice CT.

Key Words. Computed tomography; coronary artery; calcium; radiation dose.

Acad Radiol 2008; 15:958–965

[1] From the Department of Clinical Radiology, Hiroshima University Hospital, 1-2-3, Kasumi-cho, Minami-ku, Hiroshima, 734-8551, Japan (J.H., M.K., C.F., R.A.); CT Lab of Great China, GE Healthcare, Mongkok Kowloon, Hong Kong (Y.S.); GE Yokogawa Medical Systems, Ltd., Tokyo, Japan (K.S.); and Department of Molecular and Internal Medicine, Division of Clinical Medical Science (T.K., H.Y.), and Department of Radiology, Division of Medical Intelligence and Informatics (K.I.), Programs for Applied Biomedicine, Graduate School of Biomedical Sciences, Hiroshima University, Minami-ku, Hiroshima, Japan. Received December 21, 2007; accepted January 8, 2008. This study was supported by The Tsuchiya Foundation (http://www.tsuchiya-foundation.or.jp), Hiroshima, Japan. **Address correspondence to:** J.H. e-mail: horiguch@hiroshima-u.ac.jp

doi:10.1016/j.acra.2008.03.007

Coronary artery calcium (CAC) scoring is performed to evaluate the presence of coronary atherosclerosis or to assess the progression and regression of coronary atherosclerosis (1). Therefore, low variability and low radiation exposure are both key requirements on CAC scoring. Interscan variability of Agatston score (2) on electron beam computed tomography (CT), however, yielding 20% to 37% (3–6), is high, considering that normal progression of CAC scores per year is 14% to 27% (average 24%) (7) and is accelerated up to 33% to 48% with significant coronary disease (8,9). To reduce the variability, the volumetric approach (3) and the calcium mass (4) were devised as alternative CAC scoring algorithms. Also, on multidetector CT (MDCT), CAC scoring using the conventional Agatston method on nonoverlapping reconstruction yields high interscan variability: 23% to 43% (10–12) on 4-slice spiral CT and 22% (13) on 16-slice CT. Through retrospective electrocardiographically (ECG)-gated overlapping scan, a considerable reduction in interscan variability of Agatston scores can be achieved: 23% to 12% (10) and 22% to 13% (13), but at the expense of increased radiation exposure compared with ECG-triggered scan. Thin-slice images (1.25 or 1.5 mm) are shown to also reduce variability of CAC in both electron beam CT (14,15) and 64-slice CT (16). It does, however, require an increased radiation dose to maintain required image quality. In these circumstances, CAC scoring is preferably performed with a standard image thickness (2.5 or 3 mm), offering the best balance of low scoring variability and low radiation dose. The purpose of this study is, using a pulsating cardiac phantom, to assess the variability of CAC scoring on 64- and 16-slice CT scanners by both prospective ECG-triggered and retrospective ECG-gated scans.

MATERIALS AND METHODS

Cardiac Phantom

A prototype cardiac phantom is commercially available (ALPHA 2; Fuyo Corp., Tokyo, Japan). The phantom consists of five components: driver, control, support, rubber balloon, and electrocardiograph. A controller with an electrocardiographic synchronizer drives the balloon. The main characteristics of this phantom are programmable variable heart rate sequences and mimicking of natural heart movements. Details of the phantom are described elsewhere (17,18).

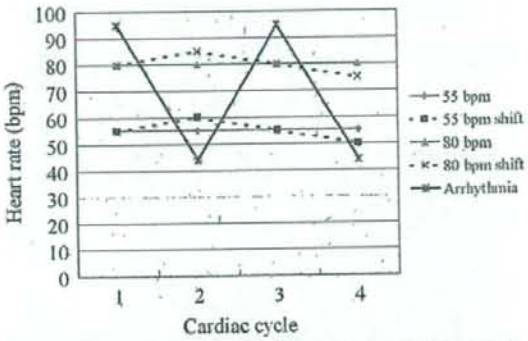

Figure 1. Heart rate sequences. The graph shows five types of heart rate sequences programmed to the electrocardiographic generator. Heart rates in the sequence "55 bpm shift" repeat a cycle of 55, 60, 55, and 50 bpm. bpm, beats per minute.

In this study, five types of heart rate sequences were programmed (Fig. 1). Two were stable heart rate sequences, two were "shift" sequences, and the remaining one was arrhythmia. The "shift" sequence was defined as heart rate with small variation, that is, the sequence "55 beat/min shift" repeats a cycle of 55 beats/min, 60, 55, and 50 beats/min. The volumes of the balloon phantom at the systolic and diastolic phases were approximately 100 and 200 ml, respectively. The main motion of the coronary artery models was in in-plane direction. Deformity of the balloon, however, resulted in some through-plane motion.

Coronary Artery Calcium Models

Three coronary artery models (plastic cylinders with a diameter of 4 mm) and different calcified plaque CT densities (silicone: ~240 Hounsfield units [HU], putty: ~600 HU, Teflon: ~1000 HU) were manufactured for this experiment (Fuyo Corp.). Each coronary artery model had four sizes of plaques: 1, 3, 5, and 10 mm in length. These plaques resulted in an 82% area of stenosis. The coronary artery models were attached to the balloon phantom (mimicking the heart) with the long axis of the model corresponding to the z-axis and were surrounded by oil (−112 HU), simulating epicardial fat (Fig. 2).

Prospective ECG-triggered Axial 64-Slice CT Protocol

Three repeated scans with a table advancement of 1 mm during the scans were performed using a 64-slice MDCT scanner (LightSpeed VCT; GE Healthcare,

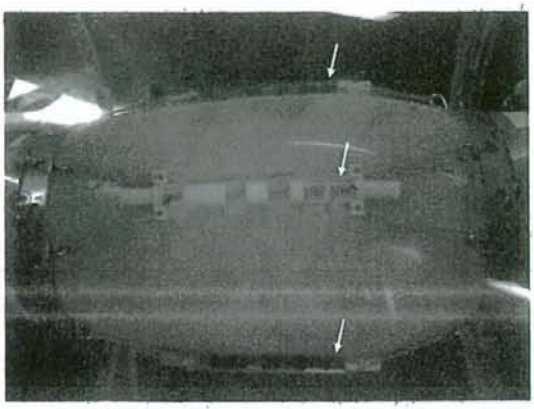

a.

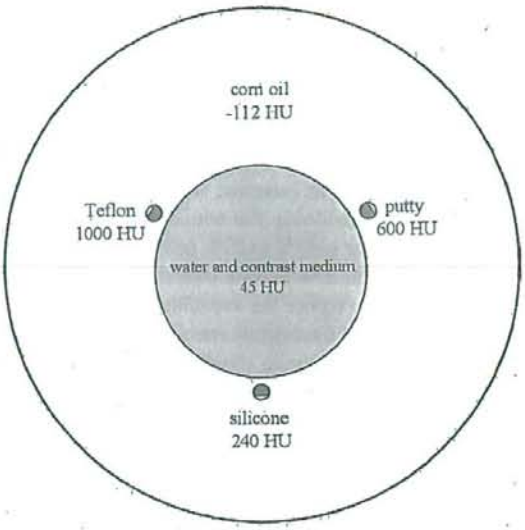

b.

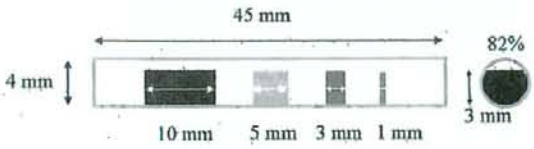

c.

Figure 2. Cardiac balloon phantom. A pulsating phantom is shown with three coronary artery models, indicated with *arrows* (**a**). The coronary artery models with different computed tomographic densities were attached to a balloon filled with a mixture of water and contrast medium (45 Hounsfield units [HU]) to simulate noncontrast blood. The balloon was submerged in corn oil (−112 HU), simulating epicardial and pericardial fat (**b**). The drawing shows four coronary artery calcium models (1, 3, 5, and 10 mm in length), resulting in 75% area stenosis, inserted into a coronary artery model with a diameter of 4 mm (**c**).

Waukesha, WI). Prospective ECG-triggered axial scan was performed using 2.5-mm collimation width × 16 detectors so that the center of the temporal window corresponded to 80% of the RR interval (diastole of the phantom). The scanning parameters were a gantry rotation speed of 0.35 s/rotation, 120 kV, and 140 mA. The matrix size was 512 × 512 pixels and the display field of view was 26 cm. The reconstruction kernel for soft tissue, which is routinely used in abdominal imaging, was used. The temporal resolution was 175 ms.

Retrospective ECG-gated Spiral 64-Slice CT Protocol

Retrospective ECG-gated spiral scan was performed with 1.25-mm collimation width × 32 detectors. The tube current was controlled using the electrocardiographic modulation technique. The maximal current was set to 140 mA during the cardiac phase 70% to 90% and was reduced in the other phase to a minimum of 30 mA. CT pitch factor was set to 0.20 by the heart rate, according to the manufacturer's recommendations for the coronary CT angiography protocol. Images of 2.5-mm thickness were retrospectively reconstructed with 1.25-mm spacing to reduce partial volume averaging. Multisector reconstruction was used on the heart rate sequences of 85 beats/min and 85 beats/min shift. The temporal resolution was 134 ms on 85 beats/min and varied on 85 beats/min shift, depending on the combination of adjacent heart rates used for image reconstruction. Other scanning parameters were the same as prospective ECG-triggered 64-slice CT protocol.

Prospective ECG-triggered Axial 16-Slice CT Protocol

A 16-slice MDCT scanner (LightSpeed Ultrafast 16; GE Healthcare) was used. Scan was performed using with 2.5-mm collimation width × 8 detectors. Gantry rotation speed was 0.5 s/rotation. The tube current of 100 mA, which is a standard level on CAC scoring using 0.5 s/rotation scanners (19), was used. The temporal resolution was 250 ms. Other scanning parameters were the same as the prospective ECG-triggered 64-slice CT protocol.

Retrospective ECG-gated Spiral 16-Slice CT Protocol

The scan was performed with 1.25-mm collimation width × 16 detectors. The electrocardiographic modulation technique was not available and the current was set to 100 mA. CT pitch factors varied from 0.275 to 0.325 by the heart rate, according to the manufacturer's recommendations for coronary CT angiography protocol. Images of 2.5-mm thickness with 1.25-mm spacing were reconstructed. Multisector reconstruction was used on the heart rate sequences of 85 beats/min and 85 beats/min shift. The temporal resolution was 158 ms on 85 beats/min and varied on 85 beats/min shift, depending on the combination of adjacent heart rates used for image reconstruction. Other scanning parameters were the same as the prospective ECG-triggered 16-slice CT protocol.

Calcium Scoring

The Agatston (2), calcium volume, and mass (4), summing over all slices corresponding to each CAC model, were determined on a commercially available external workstation (Advantage Windows Version 4.2; GE Healthcare), CAC-scoring software (Smartscore Version 3.5), and a calibrating anthropomorphic phantom (Anthropomorphic Cardio Phantom, Institute of Medical Physics, and QRM GmbH, Möhrendort, Germany) according to the following equations:

$$\text{Agatston score} = \text{slice increment/slice thickness} \times \sum(\text{area} \times \text{cofactor}) \quad (1)$$

$$\text{Volume} = \sum(\text{area} \times \text{slice increment}) \quad (2)$$

$$\text{Mass} = \sum(\text{area} \times \text{slice increment} \times \text{mean CT density}) \times \text{calibration factor (19).} \quad (3)$$

The calcium phantom was scanned on the four protocols to enable calibration for determining calcium mass. All CT scans were scored by one radiologist with eight years experience of CAC measurement. Interobserver variability was not investigated as CAC scoring in this phantom study was very simple.

Coronary Artery Calcium Score

Each of the Agatston, volume, and mass scores, in logarithmic scale to reduce skewness, were compared between the protocols using a one-factor analysis of variance (ANOVA) test. Sixty scans (4 protocols, 5 heart rate sequences, 3 repeated scans) were performed on 12 CAC materials.

Interscan Variability of Repeated Coronary Artery Calcium Scoring

The percentage variability was determined by calculating the mean numeric difference between each of the three score values and dividing this by the mean score as follows:

$$1/3 \times [\text{abs}(S1 - S2) + \text{abs}(S2 - S3) + \text{abs}(S3 - S1)]/[1/3 \times (S1 + S2 + S3)]$$

where abs is absolute value, S1 is CAC score on the first scan, and S2 and S3 are the CAC scores on the second and third scans, respectively. From the 60 scans (four protocols, five heart rate sequences, and three scans), 720 sets of variability (12 CAC materials and three scoring algorithms) data were obtained. The interscan variability was compared between the protocols and scoring algorithms using two-factor factorial ANOVA.

Interprotocol Variability of Coronary Artery Calcium Scoring

The percentage variability was determined by calculating the mean numeric difference between each of the four score values and dividing this by the mean score as follows:

$$1/6 \times [\text{abs}(S1 - S2) + \text{abs}(S1 - S3) + \text{abs}(S1 - S4) + \text{abs}(S2 - S3) + \text{abs}(S2 - S4) + \text{abs}(S3 - S4)]/[1/4 \times (S1 + S2 + S3 + S4)]$$

where abs is absolute value, and S1, S2, S3, and S4 are CAC scores on the 64-slice prospective, 64-slice retrospective, 16-slice prospective, and 16-slice retrospective, respectively. From the 60 scans, 540 sets of variability (12 CAC materials and three scoring algorithms) data were obtained. The interprotocol variability was compared between the repeated scans and scoring algorithms using two-factor factorial ANOVA.

Image Noise

Image noise, defined as standard deviation of CT value of the cardiac phantom, was measured 15 times (five heart rate sequences and three repeated scans). These val-

Table 1
Agatston, Volume, and Mass Scores on 64-Slice Prospective, 64-Slice Retrospective, 16-Slice Prospective, and 16-Slice Retrospective Scans

	64-Slice Prospective	64-Slice Retrospective	16-Slice Prospective	16-Slice Retrospective
1 mm				
Agatston	27 (37), 1–55	26 (34), 3–47	29 (37), 3–61	25 (31), 1–55
Volume	32 (37), 4–65	35 (45), 9–54	35 (39), 8–61	36 (45), 4–65
Mass	5 (6), 0–8	5 (7), 1–9	6 (7), 1–10	5 (7), 0–10
3 mm				
Agatston	79 (89), 25–121	80 (97), 22–169	92 (106), 24–187	84 (101), 19–191
Volume	75 (84), 34–106	76 (84), 37–146	87 (93), 35–172	81 (90), 31–170
Mass	15 (18), 5–23	16 (20), 5–24	19 (23), 5–33	16 (18), 4–26
5 mm				
Agatston	109 (123), 52–161	125 (140), 56–253	143 (159), 49–275	135 (150), 42–273
Volume	97 (96), 62–129	112 (115), 73–216	125 (129), 70–234	125 (129), 66–212
Mass	22 (24), 9–35	26 (30), 11–49	29 (35), 12–53	27 (32), 9–45
10 mm				
Agatston	242 (263), 120–413	233 (264), 129–395	269 (304), 107–524	260 (295), 93–441
Volume	204 (212), 139–309	199 (210), 141–288	229 (234), 145–422	223 (231), 139–342
Mass	52 (60), 21–76	53 (61), 24–77	59 (68), 24–90	55 (62), 21–85
Overall				
Agatston	114 (108), 1–413	116 (102), 3–395	133 (117), 3–524	126 (108), 1–411
Volume	102 (87), 1–441	105 (87), 9–288	119 (101), 8–422	116 (96), 4–342
Mass	24 (21), 0–76	25 (22), 1–77	28 (24), 1–90	26 (22), 0–85

64-Slice Prospective: prospective ECG-triggering scan on 64-slice CT; 1 mm: 1 mm-sized coronary artery calcium models (silicone, putty, and Teflon).
Data are expressed as mean (median), range.

ues were compared between the four protocols using a one-factor ANOVA test.

Statistical Analyses

All statistical analyses were performed using a commercially available software package (Statcel2; oms-publishing, Saitama, Japan). For statistical analyses, one-factor and two-factor factorial ANOVA (multivariate calculations) tests were used to determine differences. When statistical significance was observed by two-factor factorial ANOVA, the results were made post hoc by Scheffé's test for multiple pairwise comparisons. *P*-values $<.05$ were considered to identify significant differences.

Radiation Dose

Volume computed tomography dose index (CTDIvol) displayed on Dose Report on the CT scanner was recorded for each protocol. As dose-length product (DLP) on the phantom is not suited for simulating DLP on patients' scan, DLP is defined with the assumption that the heart ranges 12 cm in the z-axis:

$$\text{DLP (mGy} \times \text{cm)} = \text{CTDIvol (Gy)} \times 12 \text{ cm}.$$

A reasonable approximation of the effective dose (E) can be obtained using the equation (20,21):

$$E = k \times DLP$$

where E is effective dose estimate and $k = 0.017$ mSv $\times$ mGy $\times$ cm. This value is applicable to chest scans and is the average between the male and female models.

RESULTS

Coronary Artery Calcium Scores

The Agatston, volume, and mass scores on the protocols are summarized in Table 1. All calcium scores were positive. The minimal score was 1, 3, and 0.4 on Agatston, volume, and mass scores, respectively. One-factor ANOVA revealed that there was no statistical significance of log-transformed CAC scores between protocols (Agatston, $P = .52$; volume, $P = .26$; and mass, $P = .25$).

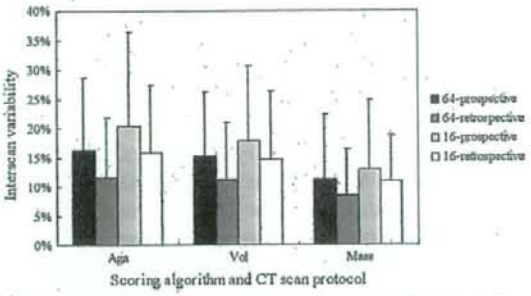

Figure 3. Interscan variability of repeated coronary artery calcium score. The graph shows the interscan variability in Agatston (Aga), volume (Vol), and mass (Mass) scoring algorithms on four protocols (16-slice prospective, *black*; 16-slice retrospective, *dark gray*; 64-slice prospective, *light gray*; 64-slice retrospective, *white*). *Bars* and *vertical lines* indicate mean and standard deviation, respectively. CT, computed tomographic.

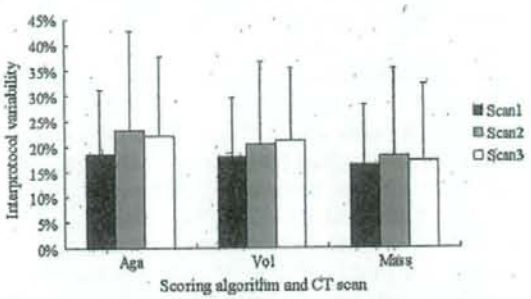

Figure 4. Interprotocol variability of coronary artery calcium score. The graph shows the interprotocol variability of CAC score on Agatston (Aga), volume (Vol), and mass (Mass) scoring algorithms. *Bars* and *vertical lines* indicate mean and standard deviation, respectively.

Interscan Variability of Repeated Coronary Artery Calcium Scoring

The interscan variability in Agatston, volume, and mass scores on the protocols are shown in Figure 3. Two-factor factorial ANOVA test revealed that there were significant differences between protocols ($P < .01$) and scoring algorithms ($P < .01$). The Scheffé test revealed that the interscan variability on 64-slice retrospective protocol was lower than that on 64-slice prospective ($P < .01$), 16-slice retrospective ($P < .01$), or 16-slice prospective ($P < .01$) protocols. The interscan variability in mass score was lower than that in Agatston ($P < .01$) or volume ($P < .01$).

Interprotocol Variability of Coronary Artery Calcium Scoring

The interprotocol variability of CAC score on Agatston, volume, and mass scoring algorithms is shown in Figure 4. Two-factor factorial ANOVA test revealed that there were no significant differences between scans ($P = .13$); however, there were significant differences between scoring algorithms ($P < .05$). The Scheffé test revealed that the interprotocol variability in mass score was lower than that in Agatston ($P < .05$) or volume ($P < .05$).

Image Noise

One-factor ANOVA revealed that image noise was different between the protocols ($P < .01$). The standard deviation of CT value on 64-slice prospective, 64-slice retrospective, 16-slice prospective, and 16-slice retrospective scans was 17.4 ± 0.5, 16.9 ± 0.7, 20.2 ± 0.7, and 22.8 ± 0.8 HU, respectively.

Radiation Dose

CTDIvol displayed on Dose Report on the CT scanner and the effective doses estimated for a typical patient were for 64-slice prospective, 2.3 mGy/0.5 mSv; 64-slice retrospective, 18.3 mGy/3.7 mSv; 16-slice prospective, 3.1 mGy/0.6 mSv; and 16-slice retrospective, 14.4 to 17.0 mGy/2.9 to 3.5 mSv (depending on the pitch).

DISCUSSION

The present study is the first to compare variability of repeated CAC scoring and radiation doses on 64-slice and 16-slice CT scanners by both prospective ECG-triggered and retrospective ECG-gated scans. The results show that retrospective ECG-gated 64-slice CT shows the lowest variability and that prospective ECG-triggered 64-slice CT, with low radiation dose, shows low variability on repeated measurement comparable to retrospective ECG-gated 16-slice CT.

The partial volume averaging is known to be a major contributor influencing interscan variability on CAC. The use of thin-slice images (14–16) or overlapping image reconstruction (10,13,22) has been suggested to reduce partial volume averaging. Some studies, however, show that thin-slice images lead to significantly increased CAC scores, due to increased noise and improved detection of subtle CAC (23,24). This indicates that thin-slice images need an increased radiation dose to maintain desirable image quality. We, therefore, decided on a slice thickness of 2.5 mm in all CT protocols. Because the purpose of CAC scoring is screening of coronary atherosclerosis or tracing its progression and regression, radiation exposure

needs to be kept "as low as reasonably achievable (ALARA)." In this respect, the effective doses of prospective ECG-triggered CT in the current study (64-slice CT, 0.5 mSv; 16-slice CT, 0.6 mSv), which are comparable to that of electron beam CT (0.7 mSv) (21), have a definite advantage over the retrospective ECG-gated scan.

CAC scores in the three scoring algorithms were not significantly different. The finding suggests that, in the CT scanner we used, CAC score did not depend on either prospective/retrospective protocol or 64-slice/16-slice CT. Concerning interscan variability of repeated CAC scores, the 64-slice retrospective scan showed the least interscan variability, implicating that this can most reliably assess the progression and regression of coronary atherosclerosis. The interscan variability on the 64-slice prospective scan also seems to be promising; it is almost the same level of the 16-slice retrospective scan. We believe that this finding is related to substantial reduction of motion artifacts, which is also one of the most important factors in increasing interscan variability on CAC. This is achieved by improved temporal resolution of 64-slice CT (175 ms for prospective ECG-triggered scan) with acceleration of gantry rotation speed. Apart from improved temporal resolution, we must also address reducing scan time, achieved by wide detector coverage. Two breath-holds, which increases variability of CAC scoring (6), are no longer necessary in most patients. Changes in heart rate and body posture are also reduced. These two factors, which increase variability, are not simulated in the present phantom study. Thus, as mentioned earlier, irrespective of whether prospective or retrospective, 64-slice CT is considered to have advantages over 16-slice CT.

Among CAC scoring algorithms, the mass showed the least variability in all CT protocols and the effect of decreasing the variability was prominent on prospective ECG-triggered scans both on 64- and 16-slice CT. Regarding interprotocol variability of CAC score, the mass showed the least variability, which best optimizes the monitoring of CAC over different CT scanners and scan protocols due to its intrinsic calibration function ability (25). The facts support the very important value of mass among CAC scoring algorithms.

High image quality on 64-slice CT, as suggested from the present study, also enhances its value. It reduces the chances of hyperdense noise being erroneously judged as calcium (26). The noise level on 16-slice CT in the study (20 HU, 23 HU) is concordant with that suggested in standardization of CAC, that is, a noise level target of 20 HU for small and medium-size patients and a noise level target of 23 HU for large patients (25). The noise level on 64-slice CT in the study (17 HU) is below the recommendation (20–23 HU). These findings indicate that further reduction of radiation dose in CAC imaging is possible, while still maintaining image quality.

The study has some limitations. We used smooth calcium models with homogeneous CT values, different from the actual calcium plaques (i.e., irregular and inhomogeneous). The heart rate sequences set were also different from those in patients. The cardiac phantom only had some through-plane motion, thus limiting the simulation of true motion of the coronary arteries. We do not, however, consider these issues important, because our purpose is not to predict variability values of the four protocols but to compare them and thereby suggest an optimal protocol. The level of variability in real patients should be further studied. The other limitation is that we did not reproduce the optimal cardiac cycle for 0.35-second rotation speed 64-slice CT. This should be verified in clinical studies by comparing multiple cardiac phase reconstruction images.

CONCLUSION

Retrospective ECG-gated 64-slice CT has the least interscan variability in repeated CAC scoring, showing the best advantage of tracking CAC amount over time. Prospective ECG-triggered 64-slice CT, with radiation doses equivalent to that of electron beam CT, shows low variability in repeated CAC scoring, comparable to retrospective ECG-gated 16-slice CT. CAC scoring with prospective ECG-triggered 64-slice CT, especially when combined with a mass algorithm, provides a balance between radiation and variability and seems optimal for clinical purposes.

REFERENCES

1. Callister TQ, Raggi P, Cooil B, Lippolis NJ, Russo DJ. Effect of HMG-CoA reductase inhibitors on coronary artery disease as assessed by electron-beam computed tomography. N Engl J Med 1998; 339:1972–1978.
2. Agatston AS, Janowitz WR, Hildner FJ, Zusmer NR, Viamonte M, Detrano R. Quantification of coronary calcium using ultrafast computed tomography. J Am Coll Cardiol 1990; 15:827–832.
3. Callister TQ, Cooil B, Raya SP, et al. Coronary artery disease: Improved reproducibility of calcium scoring with an electron-beam CT volumetric method. Radiology 1998; 208:807–814.
4. Yoon HC, Greaser LE III, Mather R, Sinha S, McNitt-Gray MF, Goldin JG. Coronary artery calcium: Alternate methods for accurate and reproducible quantitation. Acad Radiol 1997; 4:666–673.
5. Wang SJ, Detrano BC, Secci A, et al. Detection of coronary calcification with electron-beam computed tomography: Evaluation of interexamination reproducibility and comparison of three image-acquisition protocols. Am Heart J 1996; 132:550–558.

6. Achenbach S, Ropers D, Mohlenkamp S, et al. Variability of repeated coronary artery calcium measurements by electron beam tomography. Am J Cardiol 2001; 87:210–213.
7. Maher JE, Bielak LF, Raz JA, Sheedy PF II, Schwartz RS, Peyser PA. Progression of coronary artery calcification: A pilot study. Mayo Clin Proc 1999; 74:347–355.
8. Janowitz WR, Agatston AS, Viamonte M Jr. Comparison of serial quantitative evaluation of calcified coronary artery plaque by ultrafast computed tomography in persons with and without obstructive coronary artery disease. Am J Cardiol 1991; 68:1–6.
9. Fischbach R, Heindel W. Detection and quantification of coronary calcification: An update. Rofo 2000; 172:407–414.
10. Ohnesorge B, Flohr T, Fischbach R, et al. Reproducibility of coronary calcium quantification in repeat examinations with retrospectively ECG-gated multisection spiral CT. Eur Radiol 2002; 12:1532–1540.
11. Van Hoe LR, De Meerleer KG, Leyman PP, Vanhoenacker PK. Coronary artery calcium scoring using ECG-gated multidetector CT: Effect of individually optimized image-reconstruction windows on image quality and measurement reproducibility. AJR Am J Roentgenol 2003; 181: 1093–1100.
12. Daniell AL, Wong ND, Friedman JD, et al. Reproducibility of coronary calcium measurements from multidetector computed tomography. J Am Coll Cardiol 2003; 41:456A.
13. Horiguchi J, Yamamoto H, Akiyama Y, et al. Variability of repeated coronary artery calcium measurements by 16-MDCT with retrospective reconstruction. AJR Am J Roentgenol 2005; 184:1917–1923.
14. Callister T, Janowitz W, Raggi P. Sensitivity of two electron beam tomography protocols for the detection and quantification of coronary artery calcium. AJR Am J Roentgenol 2000; 175:1743–1746.
15. Vliegenthart R, Song B, Hofman A, Witteman JCM, Oudkerk M. Coronary calcification at electron-beam CT: Effect of section thickness on calcium scoring in vitro and in vivo. Radiology 2003; 229:520–525.
16. Horiguchi J, Matsuura N, Yamamoto H, et al. Variability of repeated coronary artery calcium measurements by 1.25-mm- and 2.5-mm-thickness images on prospective electrocardiograph-triggered 64-slice CT. Eur Radiol 2008; 18:209–216.
17. Horiguchi J, Shen Y, Akiyama Y, et al. Electron beam CT versus 16-MDCT on the variability of repeated coronary artery calcium measurements in a variable heart rate phantom. AJR Am J Roentgenol 2005; 185:995–1000.
18. Horiguchi J, Shen Y, Akiyama Y, et al. Electron beam CT versus 16-slice spiral CT: How accurately can we measure coronary artery calcium volume? Eur Radiol 2006; 16:374–380.
19. Hong C, Bae KT, Pilgram TK, Suh J, Bradley D. Coronary artery calcium measurement with multi-detector row CT: In vitro assessment of effect of radiation dose. Radiology 2002; 225:901–908.
20. Hunold P, Vogt FM, Schmermund A, et al. Radiation exposure during cardiac CT: Effective doses at multi-detector CT and electron-beam CT. Radiology 2003; 226:145–152.
21. Morin RL, Gerber TC, McCollough CH. Radiation dose in computed tomography of the heart. Circulation 2003; 107:917–922.
22. Kopp AF, Ohnesorge B, Becker C, et al. Reproducibility and accuracy of coronary calcium measurements with multi-detector row versus electron-beam CT. Radiology 2002; 225:113–119.
23. Achenbach S, Meissner F, Ropers D, et al. Overlapping cross-sections significantly improve the reproducibility of coronary calcium measurements by electron beam tomography: A phantom study. JCAT 2001; 25:569–573.
24. Muhlenbruch G, Thomas G, Wildberger JE, et al. Effect of varying slice thickness on coronary calcium scoring with multislice computed tomography in vitro and in vivo. Investig Radiol 2005; 40:695–699.
25. McCollough CH, Ulzheimer S, Halliburton SS, et al. Coronary artery calcium: A multi-institutional, multimanufacturer international standard for quantification at cardiac CT. Radiology 2007; 243:527–538.
26. Bielak LF, Kaufmann RB, Moll PP, MacCollough CH, Schwartz RS, Sheedy PF II. Small lesions in the heart identified at electron beam CT: Calcification or noise? Radiology 1994; 192:631–636.

Current Cardiac Imaging Reports, in press.

Prospective Electrocardiograph (ECG)-triggered Sequential Versus Retrospective ECG-Gated Spiral Computed Tomography: Pros and Cons

Jun Horiguchi, MD [1] horiguch@hiroshima-u.ac.jp
Hideya Yamamoto, MD [2] hideyayama@hiroshima-u.ac.jp
Yasuki Kihara, MD Prof [2] ykihara@hiroshima-u.ac.jp
Katsuhide Ito, MD Prof [3] hidechan@hiroshima-u.ac.jp

1) Department of Clinical Radiology, Hiroshima University Hospital
Address: 1-2-3, Kasumi-cho, Minami-ku, Hiroshima, 734-8551, Japan

2) Department of Molecular and Internal Medicine, Division of Clinical Medical Science, Programs for Applied Biomedicine, Graduate School of Biomedical Sciences, Hiroshima University
Address: 1-2-3, Kasumi-cho, Minami-ku, Hiroshima, 734-8551, Japan

3) Department of Radiology, Division of Medical Intelligence and Informatics, Programs for Applied Biomedicine, Graduate School of Biomedical Sciences, Hiroshima University
Address: 1-2-3, Kasumi-cho, Minami-ku, Hiroshima, 734-8551, Japan

Corresponding author:
Jun Horiguchi, MD
Tel: +81 82 2575257, Fax: +81 82 2575259
E-mail: horiguch@hiroshima-u.ac.jp

Abstract

Advancement of multidetector computed tomography (CT) makes it possible to visualize coronary artery as well as assessing ventricular and valvular motion, however, the necessary radiation dose is higher than that associated with X-ray coronary angiography. Recently introduced prospective electrocardiograph (ECG)-triggered CT angiography (CTA), using conventional axial scan, can markedly reduce the radiation dose, while maintaining diagnostic performance, as far as appropriately applied to selected patients. The prospective ECG-triggered CTA is technically feasible to patients with low and stable heart rate. The suitable indication is exclusion of obstructive coronary disease, rather than the analyzing of ventricular and valvular function. The scan is most beneficial for young patients, especially young women, who are at low risk of significant coronary artery disease and for whom radiation dose is of great concern.

Introduction

The diagnostic accuracy of retrospective ECG-gated 64-slice CTA, compared to coronary angiography as golden standard, is demonstrated to be high by both meta analysis [1] and prospective multicenter studies [2,3]. The major merits of this technique are low invasiveness and high negative predictive value to rule out obstructive coronary artery stenosis. This can reduce invasive coronary angiography for purely diagnostic purpose. The high radiation exposure however, being related to increasing cancerogenic risk, is a serious concern [4].

Recently introduced prospective ECG-triggered CTA, reducing radiation dose by around 80%, is gaining interest. In this article, we describe technique, radiation and associated risk, diagnostic performance and indication of prospective ECG-triggered CTA, compared to retrospective ECG-gated CTA.

1. Technical Issues

1-1. Navigator for Respiratory and Cardiac Motion

Two sources of motion, i.e. respiratory and cardiac contraction/relaxation, are associated with cardiac imaging. If the image acquisition time is longer than the patient's ability of breath-hold time, respiratory movement should be suppressed by respiratory-gating. For

typical magnetic resonance coronary angiography, navigator echoes are used to track patient's diaphragmatic motion during free-breathing. In contrast, if the data acquisition is performed within duration of one breath-hold, typically in contrast-enhanced first-pass imaging, both magnetic resonance coronary angiography and CTA (always) are obtained during a breath-hold. In this situation, ECG is mainly used in order to reduce motion artifacts from the heart (kymogram as an alternative).

1-2. Prospective ECG-triggered versus Retrospective ECG-gated Techniques

For images free of cardiac motion artifacts, acquisition times shorter than 19.1 msec are necessary [5]. Neither multidetector or electron beam CT has such a high temporal resolution, thus imaging of the heart on CT needs to appropriately fit the scan window to relatively stable timing of the heartbeat. According to Lu [6], by optimization of the cardiac phase using ECG-triggering/gating, cardiac images with the least-motion can be obtained with an acquisition time of 50-70 msec for a patient baseline heart rate of 50-100 beats per minute (bpm).

In coronary CTA, prospective ECG-triggered technique, which exposes X-ray only at a predetermined cardiac phase (usually diastolic) has been used from earlier-generation electron beam CT scanner (C-100XL, C-150XL), while the major application of this scanner is coronary artery calcium scoring. From the introduction of multidetector CT (typically 4-slice), retrospective ECG-gating, which continuously exposes X-ray with simultaneous ECG-information acquisition, thereafter, data for specific cardiac phase are used for image reconstruction, has been the mainstream in coronary CTA. Sixty-four-slice CT, and 256 or 320-slice CT, by virtue of increased coverage in the z-axis and improved temporal resolution, are drawing attention to reconsider prospective ECG-triggering.

Conventional retrospective ECG-gated scan is performed in the spiral mode using a fixed tube current throughout the cardiac cycle (Fig. 1A) and later the images are reconstructed at a specific cardiac phase(s). Depending on CT scanners, the phase(s) are quoted as a percentage of the RR interval (e.g. 75%) or as a value of absolute delay (e.g. 700msec). The cardiac phase with the least motion artifacts is known to vary for each coronary artery and between patients. In general, mid- or late-diastolic phase provides (almost) motion-free coronary artery images in low heart rate (i.e. <65 bpm). However, reconstruction at late-systolic phase becomes necessary in a higher heart rate. Searching the best phase for each coronary artery from among several phases (images are often reconstructed at 5% of RR interval) is time-consuming and effortful. For an automatic

technique, the 'Motion maps', which derives a motion strength function between multiple low-resolution reconstructions through the cardiac cycle, with periods of lowest difference between neighboring phases indicating minimal cardiac motion, has an advantage [7]. Apart from coronary artery imaging, retrospective ECG-gated scan can evaluate global and regional cardiac function (i.e. ejection fraction) and valvular morphology and function (Figure 2). Retrospective ECG-gated scan can accommodate mildly irregular heart rhythm. Using ECG-editing technique, one can arbitrarily modify the position of the temporal windows within the cardiac cycle, and correct and compensate for part or all of the artifacts produced by heart rhythm irregularities [8] (Figure 3). Thus, through data covering the entire cardiac phase, retrospective ECG-gated scan has availability in multicardiac phase reconstruction and also has the robustness for mild heart rate variation.

As a modification to conventional retrospective ECG-gated scan, current multidetector CT scanners have the option so called 'ECG-modulation', which modulates the tube current during a particular part of the cardiac cycle (Fig. 1B), allowing reduction of the radiation dose by 30% to 50% [9,10]. The extent of reduction depends on the setting of two parameters; (1) percentage of minimum tube current /maximum tube current and (2) the length of time with the minimal tube current relative to the RR interval, Systolic phase, which is not usually used in coronary artery imaging, is chosen for window at reduced current. However, cardiac function can be reasonably assessed as such high image quality in the systole is not demanded.

Prospective ECG-triggered technique, which applies radiation during short and predefined acquisition window of the cardiac cycle, has recently been devised. The R wave on the ECG is monitored; the scan starts following a time delay and stops after a certain period to resume at a similar time during the next cycle (Fig. 1C). Therefore, the image quality inherently degrades in cases of entopic beat or other arrhythmia. On 64-slice CT, step-and-shoot technique (around 4 shoots) is used to cover the entire heart. Between the adjacent X-ray exposures, one heartbeat is usual for table movement, except for low heart rate (e.g. < ** bpm), in which the table can move during X-ray-off time (systole). Regarding a disadvantage of 64-slice prospective ECG-triggered CTA, stair-step artifact, by incorrect fusion of two adjacent datasets, potential occurs and can be a reason for 'non-diagnostic' evaluability of coronary artery [11]. This can occur due to both heart rate instability and body movement. In this respect, 256 or 320-slice CT, allowing for a one-heartbeat-scan, has a definite advantage.

At least 180° of parallel-ray projections are needed to reconstruct an image. A single-source CT scanner needs half a rotation plus the fan angle (about 50° to 60°) to

deliver this amount of data, and the temporal resolution in the center of rotation is half the rotation time [12]. To reduce the radiation dose to the minimum, the least gantry rotation (230° to 240°) is used, while imaging is limited to only one cardiac phase. To accommodate some heart rate variation or to acquire broad phase data (e.g. end-systole to late-diastole) or even acquire two cardiac-cycle data (for multisegment reconstruction), one can elongate exposure time at the expense of increased radiation exposure (Fig. 1D). Some issues related to this technique remain unresolved. Most practitioners are unfamiliar with the optimal setting for X-ray exposure duration (minimal exposure time + safety margin) due to paucity of data or consensus. The optimal duration depends on several factors; (1) patient's heart rate and variation, (2) purpose of cardiac exam (coronary artery imaging or including functional analysis), (3) different gantry rotation speeds (0.27 to 0.35 sec/rotation) affecting the temporal resolution. Although complicated, to simplify and generalize this matter for practical guidance, we support adding 50 msec to the minimal exposure for coronary artery imaging, recommended by Kimura [13]. The capability in the elongation of exposure duration is different from CT scanners. Functional imaging or multi-segment reconstruction using two adjacent cardiac cycles becomes possible if the exposure duration can be set long enough. Apart from single-source CT scanner, dual-source CT, embedded with two acquisition systems mounted at an angular offset of 90° on the rotating gantry, 180° of parallel-ray geometry data can be split into two data segments of 90°. Both 90° data segments are acquired simultaneously at the same anatomical level within a quarter of the gantry rotation time (330 msec), thereby the temporal resolution is 83msec. When applying multi-segment reconstruction, the temporal resolution of 41 to 83 msec (average, 60msec) can be achieved [12].

2. Radiation Exposure

2-1. Risk Estimate

The additional lifetime risk of fatal cancer has been estimated as approximately 1 in 20,000 per mSv for the whole population by The International Commission on Radiological Protection [14]. This is also supported by The Food and Drug Administration [15]. The recent Biological Effects of Ionizing Radiation (BEIR) VII Phase 2 report [16] provided a framework for estimating lifetime attributable risk (LAR) of cancer incidence associated with radiation exposure from cardiac multidetector CT and indicated that a single population dose of 10 mSv is associated

with a LAR for developing a solid cancer or leukaemia of 1 in 1000. Therefore, CT scan needs to keep the radiation exposure "as low as reasonably achievable (ALARA)".

2-2. Radiation Exposure of Cardiac Examination

The effective doses of various CT scanners and protocols, as well as other diagnostic modalities [10,11,17-32] for comparison, are listed in Table 1. In the tradeoff of improved diagnostic capability by virtue of advances in the spatial and temporal resolution of spiral CT scanners, the radiation dose of cardiac CT examinations has increased from 4-slice to 64-slice CT. The effective dose of non-ECG-modulated 64-slice CT is high (15.2-21.4), as a commonly used pitch of 0.2 results in 80% overlap.

2-3. How to Reduce Radiation Exposure in Cardiac CT

As described earlier, ECG-modulation on retrospective ECG-gated CTA (30-50% reduction) and the use of prospective ECG-triggered CTA (77-83% reduction compared to ECG-modulated retrospective ECG-gated CTA) [24-27] are two major solutions. Low tube voltage is also effective as the radiation dose varies with the square of the kilovoltage. Decreased tube voltage increases image noise, however leads to increased opacification of vascular structures during contrast-enhanced CTA owing to an increase in the photoelectric effect and a decrease in Compton scattering [33]. Abada et al. used a tube voltage of 80 kV for 64-slice CTA and reported a dose saving of up to 88% [34]. The combination of prospective ECG-triggered CTA and 100 kV in selected patients (typically body mass index [BMI] < 25 kg x m^{-2}) succeeds in a marked reduction of radiation exposure in 64-slice CTA [11, 27-29] or dual-source CTA [30,31].

The automatic exposure control can optimize and reduce tube current. The cross section of the human body differs significantly from a circular shape, thus the attenuation of X-ray beams vary. The new online tube current modulation system takes this fact into account and automatically adjusts tube current in the x, y plane (angular modulation) or along z-axis direction, or both (combined modulation) in order to obtain constant image quality. Deetjen reported that this technique reduced the dose by 42.8% [35].

Other techniques include minimizing scan range and reducing field of view.

3. Diagnostic Performance of Prospective ECG-triggered Scan

Clinical importance of coronary CTA, which is based on evidence on retrospective ECG-gated CTA, is reported in detail elsewhere [36]. Here, we focus on the performance of prospective ECG-triggered scan.

3-1. Prospective ECG-triggered versus Retrospective ECG-gated Techniques

On 64-slice CT, a phantom study shows that prospective ECG-triggered and retrospective ECG-gated CTA have comparable performance in terms of image quality, stenosis measurement, and CT densitometry on stable heart rates up to 75 bpm [37]. The similarity on image quality and stenosis measurement has been shown in a study with the same patients' group with a heart rate < 75 bpm [24]. In different patients' groups also, image quality was reported to be similar in < 75 bpm [25]. Earls reported that prospective ECG-triggered revealed improved image quality and similar coronary artery assessability, with a heart rate < 70 pm and fluctuation < 10bpm prior to the scan [27].

Representative images on the two scan techniques obtained from the same patient are shown (Figure 4A). Prospective ECG-triggered technology is still its infancy thus there are few reports on stent imaging. In our early experience, the image quality on the two scan techniques seems to be comparable (Figure 4B). Prospective ECG-triggered scan may sometimes be advantageous as this is not inherently related to helical artifacts.

On dual-source CTA, Alkadhi reported that diagnostic image quality was obtained in around 98% of coronary artery segments (≤ 70bpm) on prospective ECG-triggered scan, which was not different from the prevalence on retrospective ECG-gated scan (> 70 bpm).

3-2. Prospective ECG-triggered versus Invasive Angiography

Similar to reported results on retrospective ECG-gated CTA, initial prospective ECG-triggered CTA studies, in selected patients with low and regular heart rate, have shown accurate diagnosis of significant (≥50%) coronary stenosis with almost 100% negative predictive value on both 64-slice CT [26,28] and dual-source CT [29] (Figure 5). It is, however, too early to conclude the value of prospective ECG-triggered CTA therefore collection of data in larger cohorts is needed.

4. Indication of Prospective ECG-triggered CTA

4-1. Technical Indication

Due to the nature of prospective ECG-triggering, scanning requires patients having a stable sinus rhythm and low heart rate [28]. The indication is considered to become stricter when we shorten X-ray exposure duration. Husmann showed that, using receiver operator characteristic curve, only 1% of coronary segments were non-diagnostic below a heart rate of 63 bpm, whereas 14.8% with heart rate of > 63 bpm ($p < 0.001$).

Although using higher temporal resolution (83 msec) on dual-source CT scanner, strict heart rate indication has been suggested. Scheffel stated that prospective ECG-triggering was feasible in selected patients with regular heart rates below 70 bpm and allows for the depiction of 98% of the coronary segments with diagnostic image quality [29]. Stolzmann showed that receiver operator characteristic analyses revealed a mean heart rate threshold for the prediction of motion artifacts of 59.9 bpm and a heart rate variability threshold for the prediction of stair-step artifacts of 2.2 bpm [30]. Gutstein recommend the indication for patients with heart rate < 65 or 70 bpm (depending on a coronary artery calcium score < or ≥ 400 HU) and a maximal heart rate variation before CTA of < 10 bpm [38].

Thus, successful prospective ECG-triggering CTA largely depends on a patient's heart rate and variability. Control of heart rate should be strict and the use of heart rate lowering drugs, such as beta blockers should be encouraged, unless contraindicated.

4-2. Clinical Indication

To reduce the radiation exposure in prospective ECG-triggered CTA, the available cardiac phase(s) would be minimized (e.g. single phase). Single-phase prospective ECG-triggered CTA appears to be the most suitable for young patients, especially young women, who are at low risk of significant coronary artery disease and in whom radiation dose is of great concern. Such a protocol might be considered appropriate as an alternative to coronary calcium scanning in circumstances in which the earliest detection of coronary atherosclerosis is desired [38].

5. Limitations of coronary CTA and Advantage of Prospective ECG-triggered CTA

According to a recent statement [36], limitations of coronary CTA include; (1) Calcifications within the coronary arteries can cause false negatives and, more frequently, false-positive findings concerning the presence of coronary artery stenosis.